European Journal of Radiology Open 3 (2016) 1–7

Contents lists available at ScienceDirect

European Journal of Radiology Open

journal homepage: www.elsevier.com/locate/ejro

Hepatocellular carcinoma: IVIM diffusion quantification for prediction of tumor necrosis compared to enhancement ratios

Suguru Kakite[a,b,1], Hadrien A. Dyvorne[b], Karen M. Lee[a], Guido H. Jajamovich[b], Ashley Knight-Greenfield[b], Bachir Taouli[a,b,*]

[a] Department of Radiology, Icahn School of Medicine at Mount Sinai, One Gustave Levy Place, New York, NY 10029, USA
[b] Translational and Molecular Imaging Institute, Icahn School of Medicine at Mount Sinai, One Gustave Levy Place, New York, NY 10029, USA

ARTICLE INFO

Article history:
Received 2 November 2015
Accepted 21 November 2015
Available online 8 December 2015

Keywords:
Hepatocellular carcinoma
Diffusion
Perfusion
Necrosis

ABSTRACT

Purpose: To correlate intra voxel incoherent motion (IVIM) diffusion parameters of liver parenchyma and hepatocellular carcinoma (HCC) with degree of liver/tumor enhancement and necrosis; and to assess the diagnostic performance of diffusion parameters vs. enhancement ratios (ER) for prediction of complete tumor necrosis.

Patients and methods: In this IRB approved HIPAA compliant study, we included 46 patients with HCC who underwent IVIM diffusion-weighted (DW) MRI in addition to routine sequences at 3.0 T. True diffusion coefficient (*D*), pseudo-diffusion coefficient (*D**), perfusion fraction (PF) and apparent diffusion coefficient (ADC) were quantified in tumors and liver parenchyma. Tumor ER were calculated using contrast-enhanced imaging, and degree of tumor necrosis was assessed using post-contrast image subtraction. IVIM parameters and ER were compared between HCC and background liver and between necrotic and viable tumor components. ROC analysis for prediction of complete tumor necrosis was performed.

Results: 79 HCCs were assessed (mean size 2.5 cm). *D*, PF and ADC were significantly higher in HCC vs. liver ($p < 0.0001$). There were weak significant negative/positive correlations between *D*/PF and ER, and significant correlations between *D*/PF/ADC and tumor necrosis (for *D*, r 0.452, $p < 0.001$). Among diffusion parameters, *D* had the highest area under the curve (AUC 0.811) for predicting complete tumor necrosis. ER outperformed diffusion parameters for prediction of complete tumor necrosis (AUC > 0.95, $p < 0.002$).

Conclusion: D has a reasonable diagnostic performance for predicting complete tumor necrosis, however lower than that of contrast-enhanced imaging.

1. Introduction

Recently, diffusion-weighted MRI (DW-MRI) has become more routinely used in the liver, with applications including tumor detection/characterization, evaluation of response to therapy, and assessment of diffuse liver disease [1–3]. Most published studies on DW-MRI have quantified the apparent diffusion coefficient (ADC) using a simple mono-exponential fit of signal intensity vs. *b* value. Pre-clinical studies in hepatocellular carcinoma (HCC) have shown that tumor necrosis yield higher ADC values compared with viable tumor components [4,5], with an observed increase in ADC after locoregional or systemic therapy [6–8]. These results have been verified in human HCC studies, which have suggested that ADC increases after therapy [9–13], or correlates with necrotic changes post therapy [14].

The diffusion signal intensity decay vs. *b* value may follow a non-monoexponential law, as there is an effect of microcirculation at low *b* value regime, which can be described by a second exponential component in the intravoxel incoherent motion (IVIM) theory proposed by Le Bihan [15], which enables calculations of true diffusion coefficient (*D*), perfusion fraction (PF or *f*), and pseudodiffusion coefficient (*D**). Recently, the IVIM model has been applied for

Abbreviations: ADC, apparent diffusion coefficient; CE T1WI, contrast-enhanced T1-weighted imaging; *D*, true diffusion coefficient ($\times 10^{-3}$ mm^2/s); *D*, *pseudodiffusion coefficient ($\times 10^{-3}$ mm^2/s); DW-MRI, diffusion-weighted MRI; IVIM, intravoxel incoherent motion; PF, perfusion fraction (%).

* Corresponding author at: Icahn School of Medicine at Mount Sinai, Translational and Molecular Imaging Institute, One Gustave Levy Place, Box 1234, New York, NY 10029, USA.
E-mail address: bachir.taouli@mountsinai.org (B. Taouli).
[1] Current address: Division of Radiology, Department of Pathophysiological and Therapeutic Science, Faculty of Medicine, Tottori University, 36-1, Nishicho, Yonago City 683-8504, Japan.

http://dx.doi.org/10.1016/j.ejro.2015.11.002

assessment of diffuse liver disease [16–20] and for characterization of focal liver lesions [21–24]. Two recent studies have investigated the role of IVIM in treated tumors [25,26]. Wagner et al. [25] (in 48 patients with 28 HCCs and 12 metastases) demonstrated significantly higher D/lower PF values in necrotic vs. viable tumor components, while ADC and D^* showed no difference. Chiaradia et al. [26] (in 15 patients with 35 colorectal cancer metastases) showed that both D ($r = 0.36$, $p = 0.035$) and ADC ($r = 0.4$, $p = 0.02$) correlated significantly with the degree of tumor necrosis.

The objectives of our study were to: (a) correlate IVIM diffusion parameters of liver parenchyma and HCC with degree of liver and tumor enhancement and necrosis; (b) assess the diagnostic performance of IVIM parameters and of enhancement ratios for prediction of complete tumor necrosis in HCC post locoregional therapy.

2. Materials and methods

2.1. Study population

Approval for this single center retrospective HIPAA compliant study was obtained from our Institutional Review Board, with a waiver for informed consent. IVIM DW-MRI was acquired in all patients undergoing routine liver MRI at 3.0 T from July 2011 through November 2011.

We applied the following inclusion criteria:

1) Adult patients (age >18 years) with chronic liver disease.
2) With untreated or treated HCC (post locoregional therapy) with a size above 1 cm.
3) Imaged on the same 3.0 T system.
4) Underwent IVIM DW-MRI and contrast-enhanced imaging.

Exclusion criteria:

1) Patients with only small HCC (size <10 mm) ($n = 8$).
2) Missing IVIM DW-MRI or contrast-enhanced imaging ($n = 4$).
3) Patients with lesions other than HCC ($n = 12$).

Seventy patients were identified, and 24 were excluded. The final patient population included 46 patients (23 men and 23 women, mean age 61 years, range 23–81 years). Forty-three patients had liver cirrhosis. The etiology of liver disease included chronic hepatitis C ($n = 34$), chronic hepatitis B ($n = 4$), NASH ($n = 2$), cryptogenic ($n = 3$), alcohol abuse ($n = 2$), autoimmune hepatitis ($n = 1$). There were 19 patients with HCC naïve to therapy, and 27 patients who underwent locoregional therapy for HCC, which included transarterial chemoembolization (TACE, $n = 17$), a combination of TACE and RFA ($n = 8$), RFA ($n = 1$) or microwave ablation ($n = 1$), with a mean/median delay of 148/100 days (range, 27–627 days) before the MRI exam.

3. MRI

MRI was performed using a 3.0 T clinical system (Discovery MR750; GE Healthcare, MW, USA) and a 32-channel torso coil. The protocol included axial fat suppressed free breathing single shot echoplanar imaging DW-MRI with diffusion gradients obtained in three orthogonal directions [TR/TE 3000/min. (55–58), flip angle 90°, 80 × 128, FOV 350–400, slice/gap 8/1.6 mm, parallel imaging ASSET factor 2, 16 b values: 0, 15, 30, 45, 60, 75, 90, 105, 120, 135, 150, 175, 200, 400, 600, 800 s/mm^2, 1 average for b 0, 15, 30 and 2 averages for the remaining b values, acquisition time 3:45 min], axial fat suppressed breath-hold FSE T2-WI (TR/TE 2800/100, 256 × 256, slice/gap 7.5/1 mm, FOV 350–400), axial and coronal SS fast spin echo T2WI (TR/TE 600/80 for coronal-240 for axial, 256 × 320, slice/gap 5/1 mm, FOV 350–400), breath-hold 2D axial in- and opposed-phase T1WI (TR/TE 3.8/2.2–1.1, flip angle 12°, 320 × 224, slice/gap 4/1 mm), and axial 3D GRE T1WI (LAVA, TR/TE 4.1/1.86, flip angle 10°, 192 × 320, slice thickness 4.4 mm, FOV 350–400 mm) before and after contrast injection [0.01 mmol/kg of gadopentetate dimeglumine (Magnevist, Bayer Healthcare Pharmaceuticals, $n = 20$) or gadobutrol (Gadavist/Gadovist, $n = 6$) and 10 mL fixed dose of gadoxetic acid (Eovist/Primovist, $n = 20$)]. Post-contrast images were obtained at the early and late arterial phases (timed using bolus tracking), portal venous phase (60 s) and late venous phase (180 s). Hepatobiliary phase images were obtained at 10 and 20 min. in patients who received gadoxetic acid.

3.1. Image analysis

3.1.1. Identification of index lesions

Two experienced observers (observer 1 and observer 2; with 13 and 9 year's experience, respectively) reviewed the images in consensus using a clinical PACS (Centricity v.3.0 GE, MW, USA). The goal of this review was to identify HCC lesions on conventional sequences. An HCC was diagnosed if the lesion fulfilled any two of the four following criteria: (1) arterial hyperenhancement, (2) portal venous or late venous washout, (3) capsule/pseudocapsule, and (4) mild to moderate hyperintensity on T2WI or high b value DW-MRI (compared with surrounding liver parenchyma) [27]. Treated HCCs were diagnosed in the presence of necrotic or partially necrotic lesions post locoregional therapy. Up to 5 lesions per patient were evaluated.

3.1.2. Assessment of tumor necrosis

The two observers measured in consensus the percentage of tumor necrosis using image subtraction with 10% increments as described previously [28]. This method has been validated against histopathology, with substantial interobserver agreement for assessment of percentage tumor necrosis (k 0.601–0.708) [28].

3.1.3. Quantitative evaluation

Observer 1 measured signal intensity (SI, au) by placing regions of interest (ROIs) within the index lesions and liver parenchyma on DW and T1WI pre- and post-contrast-enhanced images using a DICOM viewer (Osirix v.4.1.2, Pixmeo, Geneva, Switzerland). ROIs encompassed the whole lesion and were copied from contrast-enhanced images and pasted to DW images, and adjusted as needed. In large lesions (with a diameter larger than 30 mm), 3 ROIs were placed on contiguous slices and SI was averaged. Three ROIs (measuring at least 20 mm^2) were also placed within the right hepatic lobe (on 3 adjacent slices centered around the portal vein bifurcation) to measure liver SI. The left lobe of liver was not used due to cardiac motion artifacts, which can potentially alter diffusion measurement. In partially necrotic lesions, SI was measured on DW images, by placing ROIs in the necrotic and viable areas.

The mean SI of DW images was fitted to the IVIM equation [15,20] which models the SI decay with increasing b values as a fast pseudo-diffusion of constant D^* (pseudodiffusion coefficient) for the extravascular water fraction PF (perfusion fraction), and a slow molecular diffusion constant D (true diffusion coefficient) for the non-flowing spins:

$$SI_b = SI_0[PFe^{-bD*} + (1 - PF)e^{-bD}]$$

SI_b is the signal intensity (SI) at as an arbitrary b value. SI_0 is the SI in the absence of diffusion weighting ($b = 0$ s/mm^2). We used a Bayesian fitting method to estimate the IVIM parameters [20]. A Bayesian fitting method was implemented with in-house software programmed in Matlab (Matlab 2011a, Mathworks, MA, USA). ADC was calculated with mono-exponential fit by using the follow-

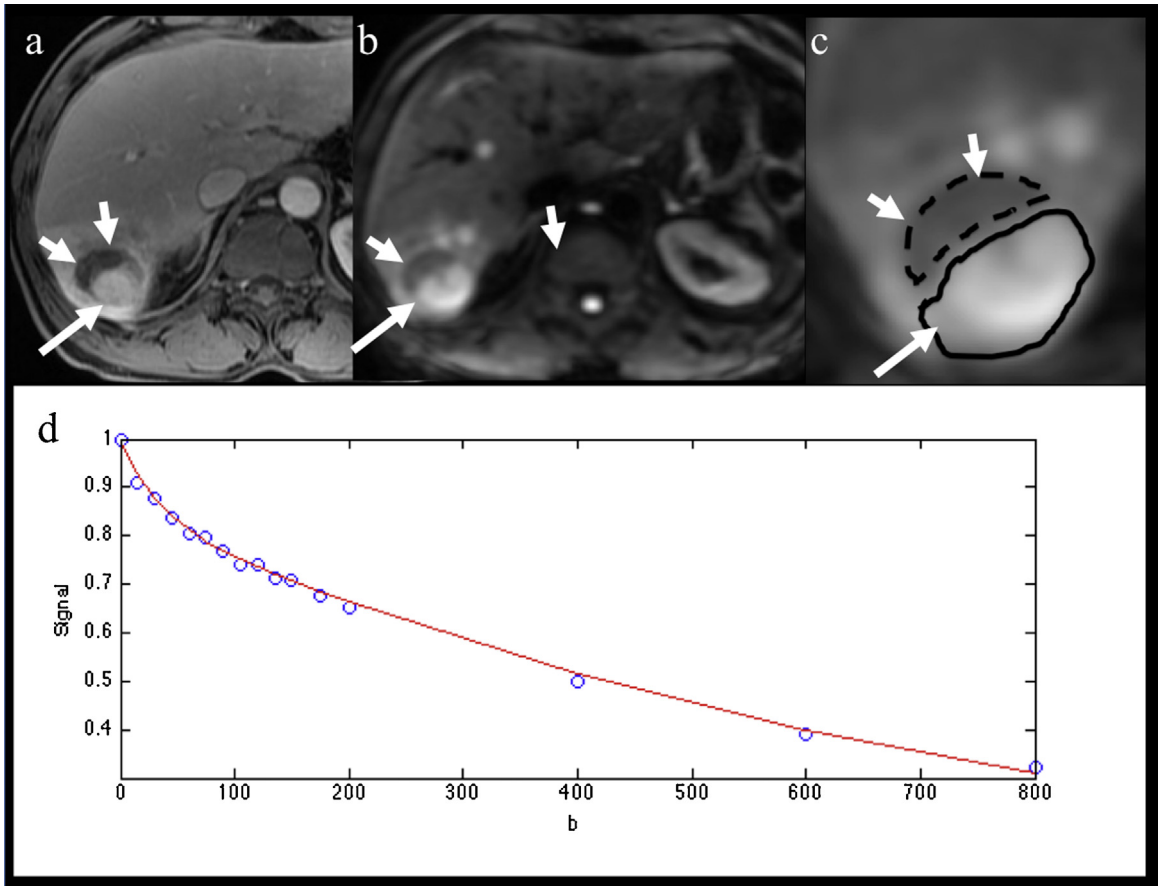

Fig. 1. 59 year-old male patient with partially necrotic HCC post TACE. (a) Axial contrast-enhanced T1 weighted image obtained at portal venous phase, (b) axial fat suppressed SS EPI DW image at b800. Both demonstrate a partially necrotic HCC with solid enhancing component with restricted diffusion (arrow) and nonenhancing necrotic component hypointense on DW-MRI (short arrows). (c) Magnified b800 DW image shows ROI placement in solid and necrotic components. (d) Fitting diffusion curve in whole HCC lesion. The following parameters were obtained in solid/necrotic HCC components/background liver: D 1.21/1.57/0.77 × 10^{-3} mm^2/s, D^* 17.53/9.44/8.03 × 10^{-3} mm^2/s, PF 15.81%/23.33%/21.58%, ADC 1.47/1.97/1.09 × 10^{-3} mm^2/s, and enhancement ratios (during portal venous phase) 113.0%/−16.4%/47.8%.

ing equation: $SI_{b1}/SI_{b2} = e^{-(b1-b2)ADC}$. We calculated the ADC value using all 16 b values. D, D^*, PF and ADC were obtained in background liver, whole HCC lesions, and in viable/necrotic components of partially necrotic lesions (Fig. 1).

Additionally, enhancement ratios (ER) were calculated in HCC (whole lesions) and liver parenchyma on dynamic post-contrast phases (2nd arterial, portal venous and late venous phases), using the following formula: ER = (SIpost – SIpre)/SIpre; where SIpost is mean SI measured on contrast-enhanced images, and SIpre is mean SI measured on unenhanced images.

3.2. Statistical analysis

Diffusion parameters were compared between tumor tissue and background liver using a non-parametric Wilcoxon signed-rank test. A Spearman correlation was performed between diffusion parameters and enhancement ratios in the liver and HCC tumors, as well as between each of diffusion parameters and enhancement ratios with% tumor necrosis. A non-parametric Mann–Whitney U test was used to compare diffusion parameters between viable and necrotic tumor compartments. ROC analysis was performed to assess the diagnostic performance of diffusion metrics vs. enhancement ratios for prediction of complete tumor necrosis (100%). Areas under the curve were compared using a DeLong test. All statistical analysis was performed using Matlab R2013b statistical toolbox.

Table 1
Diffusion parameters and enhancement ratios measured in all HCC lesions (including partially/completely necrotic and solid HCCs) and solid HCCs vs. background liver parenchyma.

	All HCCs (n = 79)	Liver parenchyma (n = 46)	p^*
D	1.128 ± 0.244	1.014 ± 0.177	**<0.0001**
D^*	41.942 ± 47.616	45.959 ± 39.932	0.64
PF	21.205 ± 10.718	14.353 ± 6.004	**<0.0001**
ADC	1.377 ± 0.280	1.152 ± 0.155	**<0.0001**
ER AP	47.50 ± 41.33	32.97 ± 18.18	**0.012**
ER PVP	47.56 ± 39.44	58.89 ± 19.21	**0.03**
ER LVP	41.06 ± 33.45	52.36 ± 16.29	**0.007**
	Solid HCCs (n = 39)	Liver parenchyma (n = 39)	p^*
D	1.047 ± 0.215	0.981 ± 0.161	0.14
D^*	52.532 ± 58.900	36.615 ± 30.810	**<0.0001**
PF	24.554 ± 11.356	17.297 ± 6.711	**<0.0001**
ADC	1.299 ± 0.240	1.141 ± 0.164	**<0.0001**
ER AP	69.75 ± 39.97	31.81 ± 16.47	**<0.0001**
ER PVP	69.09 ± 34.25	59.64 ± 16.97	**0.04**
ER LVP	56.13 ± 28.72	53.43 ± 13.88	0.74

D, true diffusion coefficient (×10^{-3} mm^2/s), D^*, pseudodiffusion coefficient (×10^{-3} mm^2/s), PF, perfusion fraction (%), ADC, apparent diffusion coefficient, ER, enhancement ratio (%), AP, arterial phase, PVP, portal venous phase, LVP, late venous phase.
Significant p-values are bolded.
* Wilcoxon signed-rank test.

Table 2
Spearman correlations between IVIM DW-MRI parameters and enhancement ratios measured with contrast-enhanced T1-weighted imaging in all HCCs. There were significant correlations between D/PF and enhancement ratios in HCC.

Liver parenchyma		ER AP (%)	ER PVP (%)	ER LVP (%)
D	*r*	0.206	0.107	0.232
	p	0.067	0.34	**0.039**
*D**	*r*	0.146	0.310	0.314
	p	0.19	**0.005**	**0.004**
PF	*r*	−0.07	−0.009	−0.018
	p	0.53	0.93	0.87
ADC	*r*	0.172	0.001	0.167
	p	0.12	0.98	0.13

HCC		ER AP	ER PVP	ER LVP
D	*r*	−0.288	−0.357	−0.344
	p	**0.009**	**0.001**	**0.001**
*D**	*r*	0.078	0.044	−0.005
	p	0.493	0.695	0.962
PF	*r*	0.364	0.309	0.281
	p	**<0.001**	**0.005**	**0.011**
ADC	*r*	−0.084	−0.167	−0.172
	p	0.45	0.139	0.128

D, true diffusion coefficient ($\times 10^{-3}$ mm^2/s), *D**, pseudodiffusion coefficient ($\times 10^{-3}$ mm^2/s), PF, perfusion fraction (%), ADC, apparent diffusion coefficient, ER, enhancement ratio (%), AP, arterial phase, PVP, portal venous phase, LVP, late venous phase.
Significant *p*-values are bolded.

4. Results

Seventy-nine HCCs (mean size 2.5 ± 2.0 cm, range 1.0–14.0 cm) were assessed in 46 patients. These included 41 untreated HCCs in 19 patients, and 38 treated HCCs in 27 patients. There were 29 patients with a single HCC evaluated, 8 with 2HCCs, and 9 with more than 2HCCs. Three patients had both untreated and treated lesions. Mean percentage necrosis on subtraction was 37.0% ± 44.5% (range, 0–100%). 19 lesions were partially necrotic (>5% necrosis), 21 were completely necrotic (100% necrosis), and 39 were solid (0% necrosis).

HCCs were diagnosed using imaging criteria in 31 patients, or histopathologically in 15 patients (with 19HCCs), by means of resection ($n = 7$), transplantation ($n = 6$) or biopsy ($n = 2$). The mean delay from MRI to pathologic confirmation was 135 days (range, 12–302 days). The delay was less than 90 days in 7 patients, precluding the use of pathologic necrosis as en endpoint. The following grade distribution was observed in pathologically confirmed lesions: well differentiated (7 lesions), well to moderately differentiated (1 lesion), moderately differentiated (8 lesions), poorly differentiated (2 lesions) and completely necrotic (1 lesion).

D, PF and ADC were all significantly higher when comparing all tumors (including partially/completely necrotic and solid HCCs) compared to background liver (Table 1), while there was no difference in *D** values. When comparing solid HCCs vs. liver, *D**/PF/ADC were all significantly higher than in liver parenchyma, while no significant difference was observed for *D* (Table 1). Enhancement ratios were significantly higher in all HCCs at the arterial phase, and significantly lower at portal venous and late venous phases compared to liver parenchyma; while solid HCCs had significantly higher enhancement ratios at the arterial and portal venous phase compared to liver parenchyma.

There were weak correlations between *D*/*D** and liver enhancement ratios at the portal venous and late venous phases (Table 2). In HCC, there were weak but significant negative/positive correlations only between D/PF and enhancement ratios. ADC did not correlate with any enhancement ratio. *D*/ADC were significantly higher in necrotic tissue compared to viable tissue; while enhancement ratios were significantly lower (Table 3, Figs. 1 and 2). There were no significant differences in PF/*D** between necrotic and viable tissue. There were significant correlations between *D*/PF/ADC and percentage tumor necrosis (Fig. 3) as follows: *D* ($r = 0.452$, $p < 0.001$), *D** ($r = -0.151$, $p = 0.18$), PF ($r = -0{,}298$, $p = 0.007$), ADC ($r = 0.346$, $p = 0.001$). The correlations between enhancement ratios and% necrosis were stronger [ER AP ($r = -0{,}683$, $p < 0.0001$); ER PVP ($r = -0{,}689$, $p < 0.0001$), ER LVP ($r = -0{,}625$, $p < 0.0001$)].

Table 3
Diffusion parameters and enhancement ratios in necrotic tumor components (including completely necrotic lesions and necrotic components of partially necrotic lesions) and viable tumor components (including viable components of partially necrotic lesions and solid lesions). There were significant differences in D/ADC and enhancement ratios between necrotic and viable components, but not in PF/D*.

	Viable tumor ($n = 58$)	Necrotic tumor ($n = 40$)	p^*
D	1.052 ± 0.231	1.299 ± 0.250	**<0.0001**
*D**	42.720 ± 51.911	27.114 ± 24.655	0.179
PF	22.373 ± 11.497	18.153 ± 8.342	0.155
ADC	1.313 ± 0.280	1.570 ± 0.334	**<0.001**
ER AP	67.15 ± 41.8	10.46 ± 14.53	**<0.0001**
ER PVP	76.3 ± 65.6	9.31 ± 18.0	**<0.0001**
ER LVP	58.3 ± 32.1	11.5 ± 17.3	**<0.0001**

D, true diffusion coefficient ($\times 10^{-3}$ mm^2/s), *D**, pseudodiffusion coefficient ($\times 10^{-3}$ mm^2/s), PF, perfusion fraction (%), ADC, apparent diffusion coefficient, ER, enhancement ratio (%), AP, arterial phase, PVP, portal venous phase, LVP, late venous phase.
Significant *p*-values are bolded.
* Mann–Whitney U test.

Table 4
ROC analysis for prediction of complete tumor necrosis using diffusion parameters and enhancement ratios. 95% confidence intervals for sensitivity and specificity are given in parentheses.

Measure	Threshold	AUC	Sensitivity (%)	Specificity (%)
D	1.15	0.811	85.7 (64.2–100)	67.2 (55.2–78.9)
*D**	22.45	0.529	44.0 (31.3–58.4)	68.9 (47.9–84.1)
PF	17.99	0.625	53.4 (40.9–67.2)	66.6 (42.6–84.2)
ADC	1.37	0.740	71.4 (47.4–88.0)	65.5 (51.7–77.0)
ER AP	22.5	0.953	86.2 (75.4–94.2)	95.2 (76.0–100)
ER PVP	25.3	0.977	94.8 (87.2–100)	90.4 (69.2–100)
ER LVP	19.8	0.972	93.1 (83.5–98.2)	95.2 (72.6–100)

D, true diffusion coefficient ($\times 10^{-3}$ mm^2/s), *D**, pseudodiffusion coefficient ($\times 10^{-3}$ mm^2/s), PF, perfusion fraction (%), ADC, apparent diffusion coefficient, ER, enhancement ratio (%), AP, arterial phase, PVP, portal venous phase, LVP, late venous phase.

Among diffusion parameters, *D* had the highest AUC (0.811) for predicting complete tumor necrosis, which was significantly higher than the AUCs achieved by PF and *D** ($p = 0.003$ and 0.026, respectively) (Table 4, Fig. 4). Enhancement ratios significantly outperformed diffusion parameters for prediction of complete tumor necrosis (AUC > 0.95, $p < 0.002$). The combination of *D* and enhancement ratio at the portal venous phase minimally improved the AUC to 0.982 without reaching significance, with sensitivity of 0.95 and specificity of 0.95.

5. Discussion

In this study, we have demonstrated that both perfusion and diffusion coefficients are higher in HCC vs. liver parenchyma when comparing a mix of treated and untreated HCCs to background liver parenchyma. This difference did not hold true for true molecular diffusion (*D*) when comparing only solid HCCs to liver parenchyma. We found weak correlations between diffusion parameters and enhancement ratios. In addition, necrotic changes post locoregional therapy were concomitant with increased *D* and ADC (apparent diffusion coefficient), without significant changes in PF (perfusion fraction). Therefore, we believe that ADC increase in tumor necrosis may be mostly attributed to an increase in true molec-

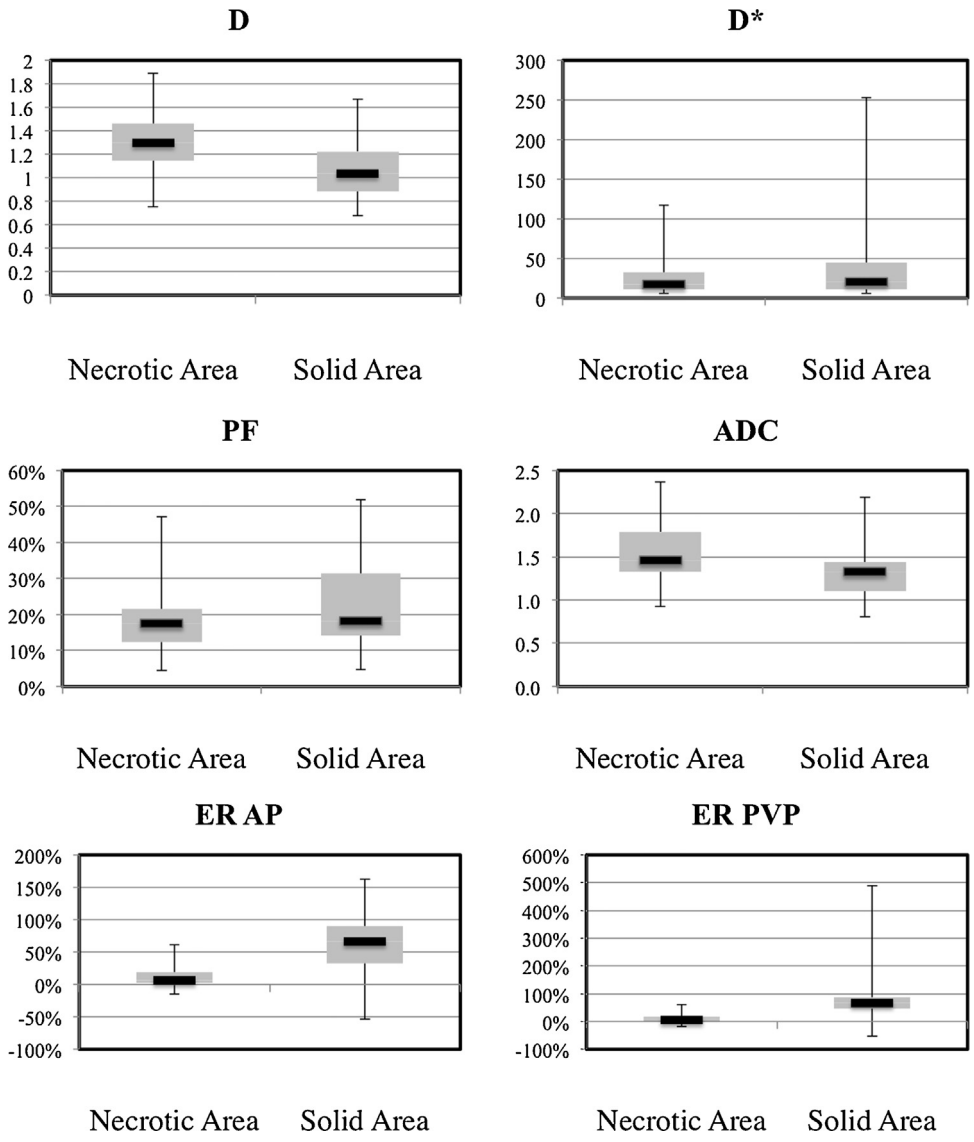

Fig. 2. Box-plot distribution of IVIM parameters and enhancement ratios (obtained during arterial and portal venous phases) in necrotic and solid HCC components.
D: true diffusion coefficient ($\times 10^{-3}$ mm^2/s), *D**: pseudodiffusion coefficient ($\times 10^{-3}$ mm^2/s), PF: perfusion fraction (%), ADC: apparent diffusion coefficient, ER: enhancement ratio (%), AP: arterial phase, PVP: portal venous phase.

ular diffusion without a significant decrease in PF. Finally, *D* had a reasonable accuracy (AUC 0.811) for predicting complete tumor necrosis, although lower than that of enhancement ratios (AUC >0.95).

The diagnosis of complete HCC tumor necrosis after locoregional therapy or lack thereof is essential, as it determines the need for additional TACE therapy or alternate treatments. Pre-clinical and clinical studies have shown that necrotic tumors yield higher ADC values compared with viable tumor components [4,5], with an observed increase in ADC after locoregional or systemic therapy [6,10,11,13]. Few studies have reported a correlation between ADC and necrosis post therapy [14]. For example, Mannelli et al. [14] reported a significant correlation between ADC and tumor necrosis post TACE assessed on liver explant ($r = 0.64$, $p < 0.001$). For pre-

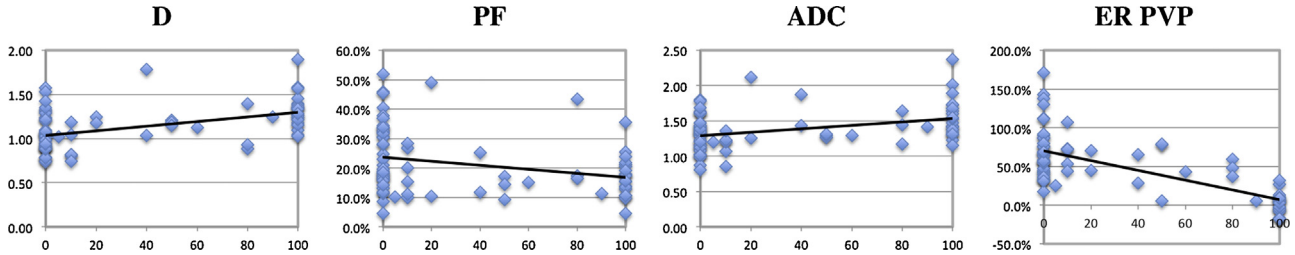

Fig. 3. Correlation plots between each of IVIM DW-MRI parameters and enhancement ratios obtained during portal venous phase (*y*-axis) with percentage tumor necrosis (*x*-axis) assessed on image subtraction.
D: true diffusion coefficient ($\times 10^{-3}$ mm^2/s), PF: perfusion fraction (%), ADC: apparent diffusion coefficient, ER: enhancement ratio (%), PVP: portal venous phase.

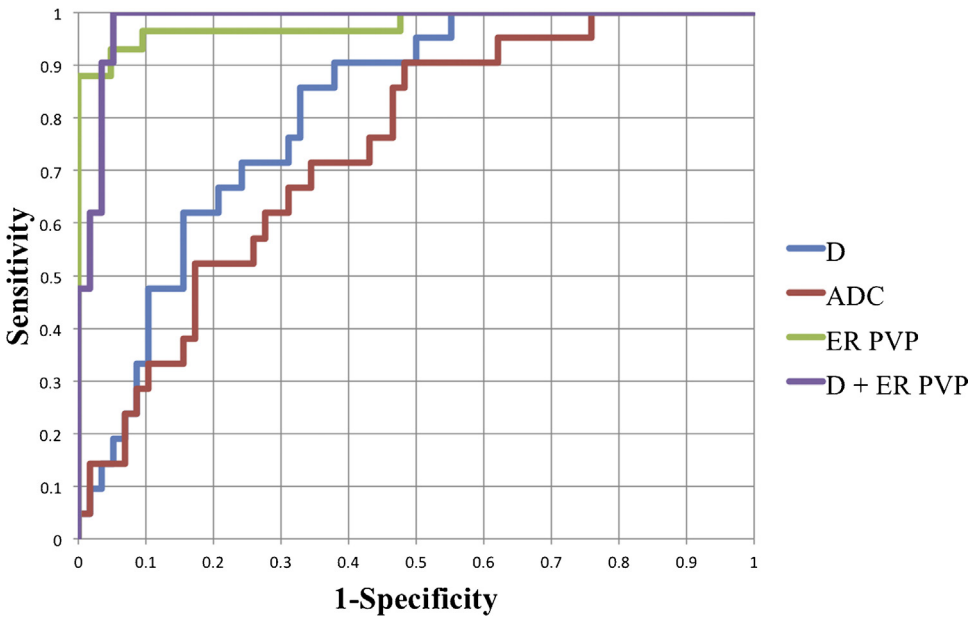

Fig. 4. ROC curves showing performances of *D*, ADC, enhancement ratio (ER) at portal venous phase, and combination of *D* + ER for prediction of complete tumor necrosis (see Table 4 for AUC values).
D: true diffusion coefficient ($\times 10^{-3}$ mm^2/s), ADC: apparent diffusion coefficient, ER: enhancement ratio (%), PVP: portal venous phase.

diction of pathologic complete tumor necrosis, the AUC of ADC was 0.85, equivalent to that of subtraction (0.82–0.89) [14]. In our study, we found a weak correlation between % necrosis and ADC ($r = 0.346$, $p = 0.001$), inferior to that reported by Mannelli et al. [14]. This could be explained by differences in the delay between treatment and imaging (38 days in the study by Mannelli vs. 148 days in the current study).

Although ADC is the most frequently used diffusion parameter outside the brain, it is a composite parameter with both diffusion and perfusion contributions. Biologically, it is more appropriate to separate the two components by using a biexponential IVIM model described in the pioneering work by Le Bihan [15]. The IVIM model has been applied for assessment of diffuse liver disease [16–20], and for characterization of focal liver lesions [21,22,24]. Investigators have used between 8 and 16 *b* values in the liver, with the highest *b* value ranging between 500 and 1000 [16–20,24–26,29]. In our study, we report *D* values similar to previously reported values in liver parenchyma [16–20,24,26,29] and HCC/liver metastases (range from literature 0.98 to 1.19×10^{-3} mm^2/s for liver cirrhosis, and $0.97–1.70 \times 10^{-3}$ mm^2/s for HCC/liver metastases) [19,24–26,29], the highest *D* values (1.70×10^{-3} mm^2/s) were reported for necrotic lesions [25]. These values are to be compared to mean *D* ($\times 10^{-3}$ mm^2/s) of 1.01 for liver and 1.052/1.299 for viable/necrotic tumors in our study. On the other hand, our reported ADC and PF values in liver parenchyma are on the lower end of the spectrum compared to other studies (range of reported ADC $1.15–1.41 \times 10^{-3}$ mm^2/s, for PF 10.7–30.8% in cirrhosis) [16–20,24,26,29]. This may be due to differences in low *b* values distribution. D* values are highly variable, with low reproducibility of this parameter recently reported [20,29]. There is a need to standardize the acquisition parameters in IVIM in order to apply this technique in the clinic.

Two recent studies have assessed the role of IVIM parameters in treated liver tumors [25,26]. Wagner et al. [25] (using 11 b values in 48 patients with 28HCCs and 12 metastases) demonstrated significantly higher D/lower PF values in necrotic vs. viable tumor components, while ADC and *D** showed no difference. Chiaradia et al. [26] (using 10 *b* values in 15 patients with 35 resected colorectal cancer metastases) showed that both *D* ($r = 0.36$, $p = 0.035$) and ADC ($r = 0.4$, $p = 0.02$) correlated significantly with the degree of tumor necrosis, while PF did not. We consider our results to be inline with these two studies, except for the fact that PF did not vary between necrotic and solid tumors. These studies and ours seem to indicate that increased ADC in necrosis is mostly due to an increase in *D*, and is less affected by PF.

Variable correlations have been observed between IVIM parameters and tissue enhancement or perfusion. Significant correlations (with *r* ranging from 0.42 to 0.70) have been reported in renal tumors [30] and HCC [24], while no correlation was observed when comparing with DCE-MRI in liver parenchyma [17]. In our study, there were modest positive correlations between PF and enhancement ratios in HCC. Interestingly, *D* had a weak but significant negative correlation with tumor enhancement, which should be verified prospectively. These modest correlations are not surprising, because the IVIM model provides pure intravascular information and DCE-MRI provides perfusion information including extravasation with a larger temporal scale. Henkelman et al. [31] suggested that IVIM does not measure tissue perfusion as does DCE-MRI, as it is more sensitive to blood volume transit through a voxel.

There are several limitations in this study. First, although the data was prospectively acquired, we did not include serial imaging pre- and post therapy, and we had variable delays between treatment and imaging. Second, we did not assess necrosis on histopathology, since only a small proportion of patients did undergo tissue sampling within 90 days after MRI ($n = 7$). Of note, image subtraction has been previously validated against histopathology [28].

In conclusion, we observed higher IVIM diffusion parameters in treated and untreated HCCs compared to liver parenchyma; weak correlations between IVIM parameters and tumor enhancement; and significant correlation between *D*/PF and degree of tumor necrosis. *D* has an acceptable AUC for prediction of complete tumor necrosis, better than that of ADC and PF, but lower than that of enhancement ratios. IVIM DW-MRI may have additional adjunct value for assessing HCC response in prospective trials and/or in patients who could not receive gadolinium contrast.

References

[1] B. Taouli, D.M. Koh, Diffusion-weighted MR imaging of the liver, Radiology 254 (2010) 47–66.
[2] D.M. Koh, D.J. Collins, Diffusion-weighted MRI in the body: applications and challenges in oncology, AJR Am. J. Roentgenol. 188 (2007) 1622–1635.
[3] N. Galea, V. Cantisani, B. Taouli, Liver lesion detection and characterization: role of diffusion-weighted imaging, J. Magn. Reson. Imaging 37 (2013) 1260–1276.
[4] J. Deng, T.K. Rhee, K.T. Sato, R. Salem, K. Haines, T. Paunesku, et al., In vivo diffusion-weighted imaging of liver tumor necrosis in the VX2 rabbit model at 1.5 Tesla, Invest. Radiol. 41 (2006) 410–414.
[5] H.C. Thoeny, F. De Keyzer, V. Vandecaveye, F. Chen, X. Sun, H. Bosmans, et al., Effect of vascular targeting agent in rat tumor model: dynamic contrast-enhanced versus diffusion-weighted MR imaging, Radiology 237 (2005) 492–499.
[6] B.J. Youn, J.W. Chung, K.R. Son, H.C. Kim, H.J. Jae, J.M. Lee, et al., Diffusion-weighted MR therapeutic evaluation after chemoembolization of VX-2 carcinoma implanted in rabbit liver, Acad. Radiol. 15 (2008) 593–600.
[7] T. Ohira, T. Okuma, T. Matsuoka, Y. Wada, K. Nakamura, Y. Watanabe, et al., FDG-MicroPET and diffusion-weighted MR image evaluation of early changes after radiofrequency ablation in implanted VX2 tumors in rabbits, Cardiovasc. Intervent. Radiol. 32 (2009) 114–120.
[8] H. Shao, Y. Ni, J. Zhang, F. Chen, X. Dai, G. Fan, et al., Dynamic contrast-enhanced and diffusion-weighted magnetic resonance imaging noninvasive evaluation of vascular disrupting treatment on rabbit liver tumors, PLoS One 8 (2013) e82649.
[9] C.Y. Chen, C.W. Li, Y.T. Kuo, T.S. Jaw, D.K. Wu, J.C. Jao, et al., Early response of hepatocellular carcinoma to transcatheter arterial chemoembolization: choline levels and MR diffusion constants—initial experience, Radiology 239 (2006) 448–456.
[10] J. Deng, F.H. Miller, T.K. Rhee, K.T. Sato, M.F. Mulcahy, L.M. Kulik, et al., Diffusion-weighted MR imaging for determination of hepatocellular carcinoma response to yttrium-90 radioembolization, J. Vasc. Interv. Radiol. 17 (2006) 1195–1200.
[11] I.R. Kamel, E. Liapi, D.K. Reyes, M. Zahurak, D.A. Bluemke, J.F. Geschwind, Unresectable hepatocellular carcinoma: serial early vascular and cellular changes after transarterial chemoembolization as detected with MR imaging, Radiology 250 (2009) 466–473.
[12] S. Bonekamp, P. Jolepalem, M. Lazo, M.A. Gulsun, A.P. Kiraly, I.R. Kamel, Hepatocellular carcinoma: response to TACE assessed with semiautomated volumetric and functional analysis of diffusion-weighted and contrast-enhanced MR imaging data, Radiology 260 (2011) 752–761.
[13] L. Mannelli, S. Kim, C.H. Hajdu, J.S. Babb, B. Taouli, Serial diffusion-weighted MRI in patients with hepatocellular carcinoma: prediction and assessment of response to transarterial chemoembolization. Preliminary experience, Eur. J. Radiol. 82 (2013) 577–582.
[14] L. Mannelli, S. Kim, C.H. Hajdu, J.S. Babb, T.W. Clark, B. Taouli, Assessment of tumor necrosis of hepatocellular carcinoma after chemoembolization: diffusion-weighted and contrast-enhanced MRI with histopathologic correlation of the explanted liver, AJR Am. J. Roentgenol. 193 (2009) 1044–1052.
[15] D. Le Bihan, E. Breton, D. Lallemand, M.L. Aubin, J. Vignaud, M. Laval-Jeantet, Separation of diffusion and perfusion in intravoxel incoherent motion MR imaging, Radiology 168 (1988) 497–505.
[16] A. Luciani, A. Vignaud, M. Cavet, J.T. Nhieu, A. Mallat, L. Ruel, et al., Liver cirrhosis: intravoxel incoherent motion MR imaging—pilot study, Radiology 249 (2008) 891–899.
[17] J. Patel, E.E. Sigmund, H. Rusinek, M. Oei, J.S. Babb, B. Taouli, Diagnosis of cirrhosis with intravoxel incoherent motion diffusion MRI and dynamic contrast-enhanced MRI alone and in combination: preliminary experience, J. Magn. Reson. Imaging 31 (2010) 589–600.
[18] B. Guiu, J.M. Petit, V. Capitan, S. Aho, D. Masson, P.H. Lefevre, et al., Intravoxel incoherent motion diffusion-weighted imaging in nonalcoholic fatty liver disease: a 3.0-T MR study, Radiology 265 (2012) 96–103.
[19] J.H. Yoon, J.M. Lee, J.H. Baek, C.I. Shin, B. Kiefer, J.K. Han, et al., Evaluation of hepatic fibrosis using intravoxel incoherent motion in diffusion-weighted liver MRI, J. Comput. Assist. Tomogr. 38 (2014) 110–116.
[20] H.A. Dyvorne, N. Galea, T. Nevers, M.I. Fiel, D. Carpenter, E. Wong, et al., Diffusion-weighted imaging of the liver with multiple b values: effect of diffusion gradient polarity and breathing acquisition on image quality and intravoxel incoherent motion parameters—a pilot study, Radiology 266 (2013) 920–929.
[21] J.H. Yoon, J.M. Lee, M.H. Yu, B. Kiefer, J.K. Han, B.I. Choi, Evaluation of hepatic focal lesions using diffusion-weighted MR imaging: comparison of apparent diffusion coefficient and intravoxel incoherent motion-derived parameters, J. Magn. Reson. Imaging 39 (2014) 276–285.
[22] S. Doblas, M. Wagner, H.S. Leitao, J.L. Daire, R. Sinkus, V. Vilgrain, et al., Determination of malignancy and characterization of hepatic tumor type with diffusion-weighted magnetic resonance imaging: comparison of apparent diffusion coefficient and intravoxel incoherent motion-derived measurements, Invest. Radiol. 48 (2013) 722–728.
[23] H. Watanabe, M. Kanematsu, S. Goshima, K. Kajita, H. Kawada, Y. Noda, et al., Characterizing focal hepatic lesions by free-breathing intravoxel incoherent motion MRI at 3.0 T, Acta Radiol. (2013).
[24] S. Woo, J.M. Lee, J.H. Yoon, I. Joo, J.K. Han, B.I. Choi, Intravoxel incoherent motion diffusion-weighted MR imaging of hepatocellular carcinoma: correlation with enhancement degree and histologic grade, Radiology 270 (2014) 758–767.
[25] M. Wagner, S. Doblas, J.L. Daire, V. Paradis, N. Haddad, H. Leitao, et al., Diffusion-weighted MR imaging for the regional characterization of liver tumors, Radiology 264 (2012) 464–472.
[26] M. Chiaradia, L. Baranes, J.T. Van Nhieu, A. Vignaud, A. Laurent, T. Decaens, et al., Intravoxel incoherent motion (IVIM) MR imaging of colorectal liver metastases: are we only looking at tumor necrosis? J. Magn. Reson. Imaging 39 (2014) 317–325.
[27] M.S. Park, S. Kim, J. Patel, C.H. Hajdu, R.K. Do, L. Mannelli, et al., Hepatocellular carcinoma: detection with diffusion-weighted versus contrast-enhanced magnetic resonance imaging in pretransplant patients, Hepatology 56 (2012) 140–148.
[28] S. Kim, L. Mannelli, C.H. Hajdu, J.S. Babb, T.W. Clark, E.M. Hecht, et al., Hepatocellular carcinoma: assessment of response to transarterial chemoembolization with image subtraction, J. Magn. Reson. Imaging 31 (2010) 348–355.
[29] S. Kakite, H. Dyvorne, C. Besa, N. Cooper, M. Facciuto, C. Donnerhack, et al., Hepatocellular carcinoma: short-term reproducibility of apparent diffusion coefficient and intravoxel incoherent motion parameters at 3.0 T, J. Magn. Reson. Imaging 41 (2015) 149–156.
[30] H. Chandarana, V.S. Lee, E. Hecht, B. Taouli, E.E. Sigmund, Comparison of biexponential and monoexponential model of diffusion weighted imaging in evaluation of renal lesions: preliminary experience, Invest. Radiol. 46 (285) (2011) 285–291.
[31] R.M. Henkelman, Does IVIM measure classical perfusion? Magn. Reson. Med. 16 (1990) 470–475.